LA-8911-MS

Nuclear-Accident Dosimetry: Measurements at the Los Alamos SHEBA Critical Assembly

University of California

LOS ALAMOS SCIENTIFIC LABORATORY
Post Office Box 1663 Los Alamos, New Mexico 87545

NUCLEAR ACCIDENT DOSIMETRY: MEASUREMENTS AT THE LOS ALAMOS SHEBA CRITICAL ASSEMBLY

by

Dennis G. Vasilik, Robert W. Martin, and Dru Fuller

ABSTRACT

Criticality dosimeters were exposed to different degraded neutron and gamma-ray energy spectra from the Los Alamos Solution High Energy Burst Assembly (SHEBA). The liquid critical test assembly was operated in the continuous mode to provide a mixed source of neutron and gamma-ray radiation for the evaluation of Los Alamos criticality detector systems. Different neutron and gamma-ray spectra were generated by operating the reactor (a) shielded by 12 cm of Lucite, (b) unshielded, (c) shielded by 20 cm of concrete, and (d) shielded by 15 cm of steel. This report summarizes the dosimetry measurements conducted for these different configurations. In-air measurements were conducted with shielded and unshielded area and personnel dosimeters. Phantom measurements were made using personnel dosimeters. Combined blood-sodium and hair sulfur activation measurements of absorbed dose were also made. In addition, indium foils placed on phantoms were evaluated for the purpose of screening personnel for radiation exposure.

I. INTRODUCTION

The Solution High Energy Burst Assembly (SHEBA), a critical test assembly, was made operational by Los Alamos researchers in 1980. The assembly has been used to provide a source of neutron and gamma-ray radiation for the testing of criticality alarm detectors and a variety of area and personnel criticality dosimeters. A number of government and private agencies have used the SHEBA to evaluate their criticality measurement devices.

SHEBA uses a liquid solution of uranyl fluoride (5% enriched uranium) as a fuel. The critical assembly vessel is a stainless steel, right-circular cylinder, 56 cm in diameter and 36.3 cm high. The Los Alamos Health Physics Group has exposed area and personnel dosimeters to mixed neutron and gamma-ray radiation from the SHEBA assembly. This Nuclear Accident Dosimetry (NAD) study provided an opportunity to expose criticality dosimeters to different degraded neutron and gamma-ray energy spectra from a liquid system. To date, many organizations have evaluated criticality dosimeters of a variety of types for fast metal reactor systems, usually in the pulsed mode. SHEBA has provided a rare opportunity to conduct dose assessments for a liquid critical assembly in the continuous mode.

This report presents the results of the Los Alamos measurements. To a large extent, the results are provided in a format developed by the Oak Ridge National Laboratory's (ORNL) Dosimetry Applications Research (DOSAR) group.[1] The object has been to conform to a standardized format in order to allow other NAD personnel the opportunity to analyze and compare their data more readily.

II. DESCRIPTION OF EXPERIMENTS

Nuclear criticality accidents were simulated by operating SHEBA in the continuous mode. Long exposure times were used to optimize measurement statistics. Dosimeters were exposed to different neutron energy spectra and neutron-to-gamma ratios. This was accomplished by operating the reactor (a) shielded by 12 cm of lucite, (b) unshielded, (c) shielded by 20 cm of concrete, and (d) shielded by 15 cm of steel. The experimental conditions are summarized in Table I. In Table II, we describe the location of the dosimeters used in these studies. The Los Alamos Criticality Dosimeter (LACD) packet is an area monitor located wherever a potential exists for a nuclear accident. The Personnel Neutron Dosimeter (PND) packet is used to estimate the neutron dose to an individual carrying the device. It is issued to persons working in all Los Alamos areas where a nuclear accident is possible.

For each experiment, a phantom filled with a saline solution, 1.5 mg ^{23}Na per ml of water, was exposed to the mixed neutron/gamma-ray radiation from SHEBA. This sodium concentration simulates the sodium content of blood. Except for experiment number 2, the phantom was located behind the shielding. All the phantoms faced the SHEBA reactor.

Measurements of ^{24}Na activation were used to estimate neutron doses. Thermoluminescent Dosimeters (TLD) were used to determine the gamma doses. TLDs were located at each of the LACD and PND locations described in Table II. For each experiment, indium foils were placed on the front, side, and back of the phantom and were evaluated for the purpose of screening personnel for neutron exposure.

For all of these experiments, the center of the SHEBA solution was located 1.24 m above the floor. All dosimeters were placed 1.24 m above the floor.

III. DOSIMETRY

A. Personnel Dosimeters

The PND packet is used to estimate the neutron dose to a person carrying the device. The elements of the PND system are given in Table III. Figure 1 is a line drawing of the PND packet.

Neutron activation analysis is used to determine the fluence of a neutron spectrum.[2]

B. Area Dosimeters

The LACD packet is an area monitor located in areas where a potential exists for a nuclear accident. The elements of the LACD packet are given in Table IV. Figure 2 is a line drawing of the LACD packet. The LACD packet is capable of providing neutron and photon dose estimates. Activation foils are used to determine the neutron dose. Gamma-ray doses

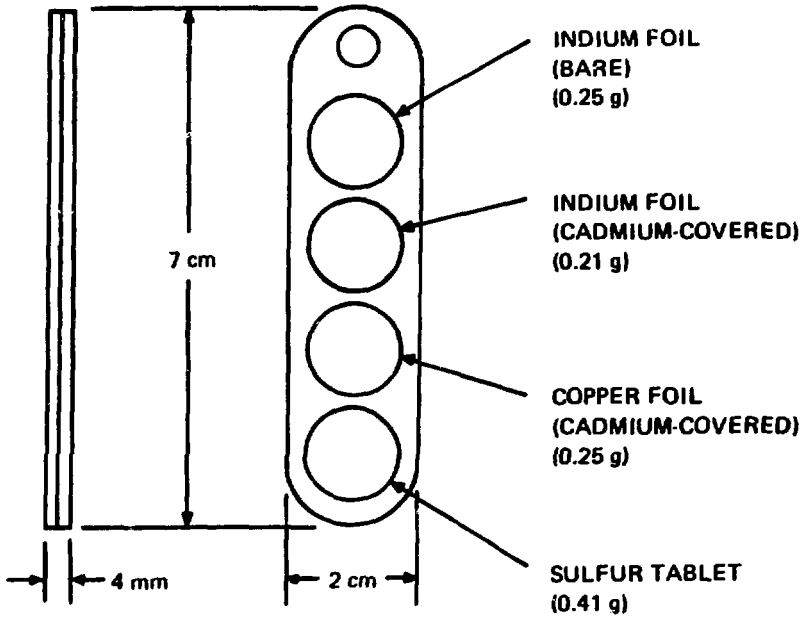

Fig. 1.
Personnel neutron dosimeter (PND) packet.

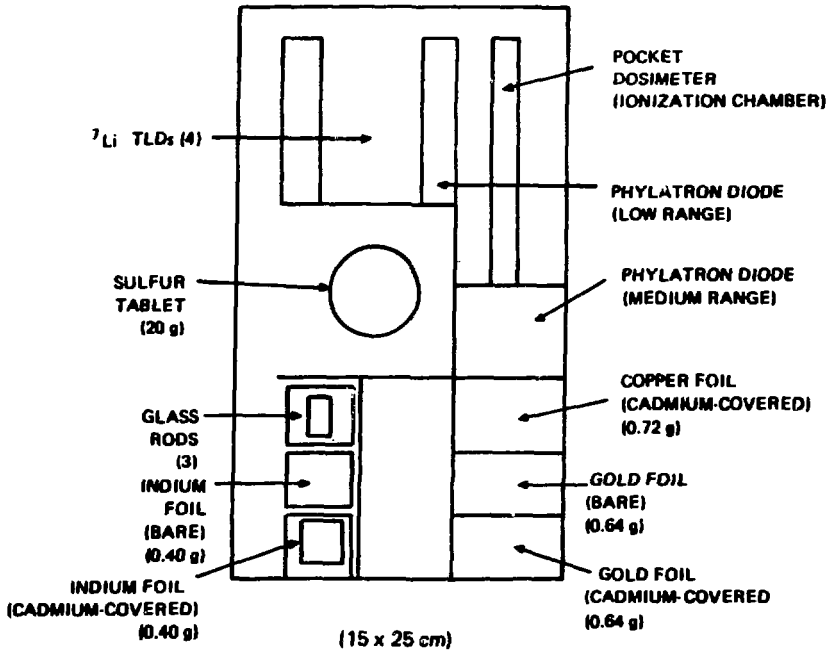

Fig. 2.
Los Alamos criticality dosimeter (LACD) packet.

are measured with TLD-700 dosimeters and silver-activated phosphate glass rods. The LACD packet is described in detail in the literature.[2] The LACD packet provides a crude estimate of the neutron spectrum.

The determination of the dose that an individual receives in a criticality accident depends on several parameters. In general, one requires a knowledge of the general shape of the neutron energy spectrum incident on the body. If the spectral shape can be estimated, then systems such as the LACD and PND packets can be used to provide accurate dose estimates[2] as suggested by IAEA* guidelines.[3] IAEA suggests an accuracy of 50% in the dose determination within 24 hours and 25% within 4 days. If the spectral shape cannot be estimated, then great difficulties can prevail in the determination of the dose. Factors that affect the neutron energy spectrum and hence the activation of threshold foils include the configuration of the source material, the position of the shielding (was it between the source and the person?), the location of the person with respect to floors, walls, and equipment, and the orientation of the person.

C. Body-Sodium Analysis

In the event that an individual might not have worn a dosimeter, or an area dosimeter might not be retrievable, the Laboratory also uses an additional technique to determine the neutron dose which depends on a combination of blood- and hair-activation. Blood-sodium activation is a well-known technique for determining the dose from a criticality accident.[4] The activation of hair sulfur is also a well-known technique for determining the neutron dose.[5-7] Hankins has shown[8] that the ratio of hair sulfur fluence to blood-sodium activation as a function of blood-sodium activation can result in dose estimates that are accurate to within ± 20-30%. This technique is independent of the neutron energy spectrum, individual orientation, neutron scattering, and shielding (except for massive metal shields). In combination with the results of PND and/or LACD dosimetry, this technique can provide accurate dose assessments of a potential criticality accident. For these experiments, sulfur tablets are used to determine the neutron fluences. Hair also can provide a good

*International Atomic Energy Agency.

estimate of the sulfur fluence. Hair would be used in the case of an exposed person who did not wear a dosimeter that included sulfur.

D. Personnel Dosimeter Screening

Early screening of potentially exposed individuals can be accomplished by determining the activity of the indium foils in a PND packet with a Geiger-Müeller instrument. The measured dose-rate from the indium in mR/hr (corrected for decay time since exposure) can be related to the neutron dose with appropriate calibration factors. Indium activation studies have been conducted for a large number of critical assemblies.[4] If the critical excursion is similar to an excursion from one of the assemblies studied, the neutron dose could be estimated to within ± 50%. Any indium activation is usually a sign that an individual involved in a criticality accident has been exposed to neutrons. Screening could be a valuable tool for determining response priorities in a criticality accident.

IV. RESULTS

A. Neutron Dosimetry

Table V shows the threshold detectors that are used in the PND and LACD packets. The particular reactions of interest and the applicable energy ranges for fluence determinations are shown. The threshold detectors are treated as if they were ideal detectors with defined thresholds, E_{th}, and with only one cross section, σ. If one knows the shape of the neutron energy spectrum, then the effective cross section, σ, for the detector is defined[9] by

$$\bar{\sigma} = \frac{\int_{E_o}^{\infty} \frac{dN}{dE}(E)\sigma(E)dE}{\int_{E_{th}}^{\infty} \frac{dN}{dE}(E)dE} , \qquad (1)$$

where

$\bar{\sigma}$ = the effective cross section for the detector,

$\frac{dN}{dE}(E)$ = the irradiating neutron energy spectrum,

$\sigma(E)$ = the detector cross section,

E_o = the absolute threshold energy for the detector, and

E_{th} = the effective threshold energy that one chooses for the detector.

For these studies, appropriate energy spectra for the configurations considered were available[10] to determine the effective cross sections. The neutron fluence, $\emptyset$, in each energy interval is determined from the activation produced in each foil as a function of the appropriate effective cross section.[2]

The neutron dose determination (absorbed dose, first collision dose, or Kerma dose in tissue) is made by multiplying the fluence in each energy region by the appropriate fluence-to-dose conversion factor and summing the individual doses. The uncertainty associated with a measurement of a neutron dose will be directly proportional to the uncertainties associated with the effective cross sections.

In Figure 3 we show

1. the absorbed dose[11] for a homogeneous anthropormorphic phantom that is a right circular cylinder with a radius r = 15 cm and a height h = 60 cm (the phantom is composed of H, C, N, and O in the proportions of a standard man,[12] and the absorbed dose is for volume Element 57 of the phantom);
2. the first collision dose[12] for soft tissue; and
3. the Kerma dose[13] for soft tissue.

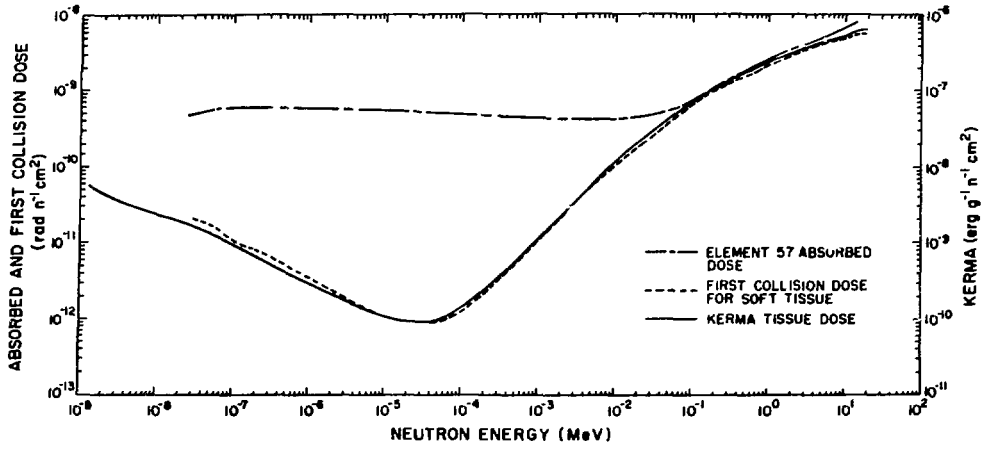

Fig. 3.
Variation of dose with neutron energy.

Absorbed dose and first collision dose must have the units of rads, whereas tissue Kerma dose is always reported as $erg \cdot g^{-1}$. Appropriate fluence-to-dose conversion factors used in this report were determined by a weighting technique described by

$$\overline{DF} = \frac{\int_{E_1}^{E_2} \frac{dN}{dE}(E)DF(E)dE}{\int_{E_1}^{E_2} \frac{dN}{dE}(E)dE},$$

where

DF(E) = appropriate fluence-to-dose conversion factor as a function of energy,

$\frac{dN}{dE}(E)$ = irradiating neutron energy spectrum (n/cm^2 - MeV), and

$\overline{DF}$ = effective fluence-to-dose conversion factor for the neutron energy range from E_1 to E_2.

1. In-Air Unshielded Results.

In-air measurements of the neutron fluence and dose were conducted with LACD and PND packets as described in Table II. Measurements were made with the dosimeters unshielded for each experiment. Both LACD and PND packets were used in order to determine how effectively the different dosimeters were able to measure the same neutron energy spectrum. In Tables VI to XI we summarize the unshielded, in-air measurements for experiments 1-4. We report the effective cross sections used for the components of the dosimeters and the reaction rates for each activation foil. The measured reaction rate represents the total number of atoms activated during a given exposure time. The reaction rate is presented in terms of $\phi\bar{\sigma} \times 10^{10}$ atoms per kW-min for each activation foil. The data of Tables VI to XI are normalized to a distance of 3 m to facilitate comparison of the results from run to run. In Table XII we show the average reaction rate for all experiments for each activation foil. The reported uncertainty represents the 1σ standard deviation of the mean. Also reported are the average reaction rates for the LACD and PND dosimeters, respectively, and the ratio of the PND to the LACD reaction rates for each activation foil. It can be observed that the LACD and PND packets are estimating the normalized reaction rates per energy group within $\pm$ 20% of the mean.

This standard deviation is considered to be a measure of agreement among individual measurements (precision). It is not a measure of accuracy which is based on precision and measurement bias. The accuracy of these measurements is strongly dominated by the uncertainty associated with the estimation of appropriate cross sections. Because the bias was not evaluated for these studies, the experimental results are not necessarily accurate. However, these studies are a necessary contribution to the data base that is available for the continued development and evaluation of NAD systems.

The data in Tables VI to XI were used in conjunction with appropriate absorbed dose-to-fluence conversion factors to determine the normalized dose-rate at 3 m from the center of the SHEBA vessel. This value is equal to 2.8 $\pm$ 0.3 rad per kW-min. This value represents the mean normalized dose-rate and the 1σ standard deviation of the mean for the LACD and PND measurements. This precision is about $\pm$ 11%. The ratio of the PND to LACD dose-rates was determined to be equal to 0.93.

In Table XIII we show the absorbed neutron dose, gamma dose, and neutron-to-gamma dose ratios for all the unshielded, in-air measurements. The mean and 1σ uncertainty associated with the determination of the neutron-to-gamma dose ratio is equal to 1.34 $\pm$ 0.08. This represents a precision of 6%. All dose estimates of Table XIII are those values measured at the position of the dosimeters.

2. In-Air, Shielded Results.

LACD packets were also placed behind the shields as described in Table II. In Tables XIV - XVI we summarize the shielded, in-air measurements for experiments 1, 3, and 4. We report the effective cross section used for the components of the LACD and the reaction rate for each activation foil. The reaction rates are those measured at the dosimeter locations. In Table XVII, we show the neutron absorbed dose, gamma dose, and neutron-to-gamma dose ratios for the in-air measurements behind the various shields. In Table XVIII, we show the ratio of the shielded to the unshielded neutron doses for experiments 1, 3, and 4. This table reflects the dose attenuation factors for the various shields considered.

3. Phantom Dose Evaluations.

For each experiment, PND packets were placed at various phantom locations. Neutron absorbed dose measurements were made at the locations described in Table II for the purpose of determining the effect of orientation of the PNDs on the phantom to a neutron

spectrum. In Tables XIX - XXIX we summarize the PND measurements on the phantoms. We report the effective cross section used for each component of the PND and the reaction rate for each activation foil. The reaction rates are those measured at the given dosimeter locations. The reaction rates for all PNDs placed on the chest of the phantom have been corrected for neutron backscatter. When appropriate neutron fluence-to-absorbed dose correction factors are applied to these data, the resulting doses are the actual doses to the phantom. We report Element 57 doses. Neutron albedo factors were calculated, based on a comparison of in-air and phantom chest fluence data. The calculated albedo factors compared very well with reported values for the appropriate boundary conditions.[14-17]

In Table XXX we show the PND packet results for the neutron absorbed dose to the phantom chest for each experiment. Also shown are the neutron absorbed doses to the phantom determined by in-air measurements with the LACD packet. Gamma doses were determined at most PND locations using the TLDs in the LACD packets and are shown in Table XXX. No corrections due to the presence of the phantom were applied to PND data for the dosimeters placed on the side and back of the phantom. In Table XXXI we show the ratios of the doses measured at the side and back of the phantom to the dose at the front of the phantom for each experiment. Ratios are presented for both the neutron and gamma dose components.

4. Body Sodium Analysis.

Los Alamos blood-sodium analyses (simulated by Na in the phantoms) were conducted for each experiment. A summary of the blood-sodium analyses is presented in Table XXXII. In Table XXXIII we show a comparison of blood-sodium dose estimates with in-air (LACD) absorbed dose determinations. Also shown is the ratio of LACD and Phantom chest (PND) absorbed dose measurements for each experiment. The excellent correspondence between the blood-sodium and LACD/PND neutron dose estimates leads us to believe that the accuracy of our measurements is within the $\pm$ 25% recommended by the IAEA.[3] These

blood-sodium results strongly support the work of Hankins.[8] A combination of blood and sulfur tablet/hair activations can be used to determine the neutron dose. For these experiments hair samples were attached to various locations on the phantoms. The sulfur fluences determined from the hair activations were within ± 15% of the sulfur fuences determined with the LACD or PND sulfur tablets.

5. Personnel Dosimeter Screening Analysis.

For each experiment, PND packets were placed on the phantoms for the purpose of evaluating indium activation for personnel exposure screening. In Table XXXIV we summarize the results of the Geiger counter readings of the indium foil in the PND packets. All these data were acquired with a LUDLUM 14C G-M meter, with a closed shield, in contact with the indium foil. All readings are corrected to the time of end of exposure. All foils decayed with a 54-min half-life, which is characteristic of ^{116m}In decay. The G-M/dose-rate-to-rad-neutron ratios are based on the LACD dosimetry of Tables XIII and XVII.

B. Gamma Dosimetry.

Gamma dose is measured primarily with thermoluminescent dosimeters (TLD). Only the LACD dosimeter includes the TLD devices. Harshaw TLD-700 LiF chips (0.32 by 0.32 by 0.09 cm) are used. The TLD-700 dosimeters contain 0.007% Li-6 and 99.993% Li-7. The TLD-700 has a very low neutron sensitivity.[18] The TLD-700 dosimeters are located inside a plastic disk for protective purposes. Photon doses can be measured from 25 millirads to about 10^4 rads with an accuracy of 10%. Standard calibration curves are used to relate photon dose to the light units determined with a TLD reader.

The gamma dosimetric results for these studies have been included in the Sec. IV. A. for ease of presentation.

V. DISCUSSION

These studies have resulted in the generation of an extensive data base for the dosimetric evaluation of a liquid critical assembly. We have demonstrated some of the capabilities and advantages of the methods used at Los Alamos for criticality dosimetry. None of the systems rely on elaborate computational or experimental programs.[2]

Per cent standard deviations for dose measurements considered in this study are within recommended IAEA limits. They are also within nuclear criticality accident standards and criteria, which state[19,20] that gamma dose should be measured to $\pm$ 20% and that neutron dose should be measured to within 25% (accuracy). However, in this study the standard deviation from the mean is a measure of precision and not accuracy. Accuracy was not determined for this study but is known to be primarily dependent upon the uncertainty associated with the determination of appropriate cross sections for a given configuration. The excellent agreement between blood-sodium dose determinations and LACD/PND evaluations strongly supports the applicability of the effective cross sections used in this study. However, improvements in measurement accuracy can result only from continued studies of NAD systems, analysis techniques, and various fissile systems.

ACKNOWLEDGEMENTS

We are grateful to Richard E. Malenfant and Harry M. Forehand of the Los Alamos Critical Experiments and Diagnostics Group for their technical support and coorperation. We also wish to thank Arthur H. Morgan III of the Los Alamos Health Physics Group for his support.

TABLE I

SHEBA EXPERIMENTAL CONFIGURATIONS

Experiment Number	Shield Configuration	Source-to-Shield Distance (m)	SHEBA Power (kilowatts)	Exposure Time (min)	Fissions	Source-to-Phantom Midpoint Distance (m)
1	12-cm Lucite	2	0.79	100	1.56×10^{17}	3.1
2	Unshielded	-	1.58	50	1.52×10^{17}	3.1
3	20-cm Concrete	2	1.49	100	2.94×10^{17}	3.1
4	15-cm Steel	4.2	1.51	100	2.99×10^{17}	4.7

TABLE II

LOCATIONS OF LACD AND PND PACKETS FOR EACH EXPERIMENTAL CONFIGURATION

Experiment Number	LACD Description	Source-to-LACD Distance (m)	PND Description		Source-to-PND Distance (m)[a]
1	(a) In-air, Unshielded	3	(a) Phantom Chest	Shielded	3
	(b) In-air, Shielded	3	(b) Phantom Back	Shielded	3.2
2	(a) In-air, Unshielded	3	(a) Phantom Chest	Unshielded	3
			(b) Phantom Side	Unshielded	3.1
			(c) Phantom Back	Unshielded	3.2
3	(a) In-air, Unshielded	3	(a) Phantom Chest	Shielded	3
	(b) In-air, Shielded	3	(b) Phantm Side	Shielded	3.1
			(c) Phantom Back	Shielded	3.2
			(d) In-air, Unshielded		2
4	(a) In-air, Unshielded	4.6	(a) Phantom Chest	Shielded	4.6
	(b) In-air, Shielded	4.6	(b) Phantom Side	Shielded	4.7
			(c) Phantom Back	Shielded	4.8
			(d) In-air, Unshielded		4.2

[a]All distances measured from center of SHEBA to dosimeter.

TABLE III

COMPONENTS OF PND PACKET

Dosimeter	Energy Range
Bare indium foil	0.025 - 0.5 eV
Cadmium-covered indium foil	0.5 - 2.0 eV and 1 - 9 MeV
Cadmium-covered copper foil	10^{-5} - 1 MeV
Sulfur tablet	2.9 - 9 MeV

TABLE IV

COMPONENTS OF LACD PACKET

Dosimeter	Energy Range
Bare indium foil	0.025 - 0.5 eV
Cadmium-covered indium foil	0.5 - 2.0 eV and 1 - 9 MeV
Bare gold Foil	0.025 - 0.5 eV
Cadmium-covered gold foil	0.5 - 10.0 eV
Cadmium-covered copper foil	10^{-5} - 1 MeV
Sulfur tablet	2.9 - 9 MeV
Phylatron diode	0.4 - 9 MeV
Thermoluminescent dosimeters (TLD-700)	0.005 - 15 MeV
Glass rod dosimeter	0.005 - 15 MeV

TABLE V

PND AND LACD DOSIMETER THRESHOLD FOILS

Number	Foil Type	Packet Type	Energy Range	Nuclear Reaction of Interest
1.	Cadmium-Covered Indium	PND and LACD	1 - 9 MeV	$^{115}_{49}In + ^{1}_{0}n \rightarrow ^{115m}_{49}In + ^{1}_{0}n' + \gamma's$
2.	Sulfur Tablet	PND and LACD	2.9 - 9 MeV	$^{32}_{16}S + ^{1}_{0}n \rightarrow ^{32}_{15}P + ^{1}_{1}p$ $^{32}_{15}P \xrightarrow[\beta^-]{} ^{32}_{16}S$
3.	Cadmium-Covered Copper	PND and LACD	10^{-5} - 1 MeV	$^{63}_{29}Cu + ^{1}_{0}n \rightarrow \left(^{64}_{29}Cu\right)^{*} \rightarrow ^{64}_{28}Ni + \gamma's$
4.	Bare Indium Cadmium-Covered Indium	PND and LACD	Thermal and Epithermal	$^{115}_{49}In + ^{1}_{0}n \rightarrow \left(^{116m}_{49}In\right)^{*} \xrightarrow[\beta^-]{} ^{116}_{50}Sn + \gamma's$
5.	Bare Gold Cadmium-Covered Gold	LACD	Thermal and Epithermal	$^{197}_{79}Au + ^{1}_{0}n \rightarrow \left(^{198}_{79}Au\right)^{*} \rightarrow ^{198}_{80}Hg + \gamma's$

TABLE VI

EXPERIMENT NUMBER 1: LACD COMPONENTS

IN-AIR, UNSHIELDED
EFFECTIVE CROSS SECTIONS AND REACTION RATES
AT 3 m FROM CENTER OF SHEBA

Detector Component	Effective Cross-section $\bar{\sigma}(cm^2)$	Energy Range	Reaction Rate $\left(\frac{\bar{\sigma} \times 10^{10} \text{ Atoms}}{kW\text{-Min}}\right)$
Bare Gold	1.07×10^{-22}	Thermal	2.4×10^{-4}
Cadmium-Covered Gold	1.55×10^{-21}	Epi-Thermal 0.62-10 eV	2.3×10^{-4}
Bare Indium	1.96×10^{-22}	Thermal	4.7×10^{-4}
Cadmium-Covered Indium (n,γ)	2.60×10^{-21}	Epi-Thermal 0.62-2 eV	4.3×10^{-4}
Cadmium-Covered Copper	2.55×10^{-25}	10^{-5}-1MeV	1.6×10^{-6}
Cadmium-Covered Indium (n,n')	2.50×10^{-25}	1-9 MeV	1.1×10^{-6}
Sulfur	2.80×10^{-25}	2.9-9 MeV	3.0×10^{-7}

TABLE VII

EXPERIMENT NUMBER 2: LACD COMPONENTS

IN-AIR, UNSHIELDED
EFFECTIVE CROSS SECTIONS AND REACTION RATES
AT 3 m FROM CENTER OF SHEBA

Detector Component	Effective Cross-section σ (cm^2)	Energy Range	Reaction Rate $\left(\frac{\sigma \times 10^{10} \text{ Atoms}}{\text{kW-Min}}\right)$
Bare Gold	1.07×10^{-22}	*Thermal*	3.5×10^{-4}
Cadmium-Covered Gold	1.55×10^{-21}	Epi-Thermal 0.62-10 eV	3.7×10^{-4}
Bare Indium	1.96×10^{-22}	Thermal	6.4×10^{-4}
Cadmium-Covered Indium (n,γ)	2.60×10^{-21}	Epi-Thermal 0.62-2 eV	6.1×10^{-4}
Cadmium-Covered Copper	2.55×10^{-25}	10^{-5}-1MeV	1.6×10^{-6}
Cadmium-Covered Indium (n,n')	2.50×10^{-25}	1-9 MeV	1.6×10^{-6}
Sulfur	2.80×10^{-25}	2.9-9 MeV	4.8×10^{-7}

TABLE VIII

EXPERIMENT NUMBER 3: LACD COMPONENTS

IN-AIR, UNSHIELDED
EFFECTIVE CROSS SECTIONS AND REACTION RATES
AT 3 m FROM CENTER OF SHEBA

Detector Component	Effective Cross-section σ (cm^2)	Energy Range	Reaction Rate $\left(\frac{\sigma \times 10^{10} \text{ Atoms}}{\text{kW-Min}}\right)$
Bare Gold	1.07×10^{-22}	Thermal	3.6×10^{-4}
Cadmium-Covered Gold	1.55×10^{-21}	Epi-Thermal 0.62-10 eV	3.6×10^{-4}
Bare Indium	1.96×10^{-22}	Thermal	5.7×10^{-4}
Cadmium-Covered Indium (n,γ)	2.60×10^{-21}	Epi-Thermal 0.62-2 eV	6.0×10^{-4}
Cadmium-Covered Copper	2.55×10^{-25}	10^{-5}-1MeV	2.1×10^{-6}
Cadmium-Covered Indium (n,n')	2.50×10^{-25}	1-9 MeV	1.3×10^{-6}
Sulfur	2.80×10^{-25}	2.9-9 MeV	4.9×10^{-7}

TABLE IX

EXPERIMENT NUMBER 3: PND COMPONENTS

IN-AIR, UNSHIELDED
EFFECTIVE CROSS SECTIONS AND REACTION RATES
AT 3 m FROM CENTER OF SHEBA

Detector Component	Effective Cross-section $\bar{\sigma}$ (cm^2)	Energy Range	Reaction Rate ($\bar{\sigma} \times 10^{10}$ Atoms / kW-Min)
Bare Indium	1.96×10^{-22}	Thermal	3.6×10^{-4}
Cadmium-Covered Indium (n,γ)	2.60×10^{-21}	Epi-Thermal 0.62-2 eV	5.0×10^{-4}
Cadmium-Covered Copper	2.55×10^{-25}	10^{-5}-1 MeV	1.8×10^{-6}
Cadmium-Covered Indium (n,n')	2.50×10^{-25}	1-9 MeV	1.1×10^{-6}
Sulfur	2.80×10^{-25}	2.9-9 MeV	5.5×10^{-7}

TABLE X

EXPERIMENT NUMBER 4: LACD COMPONENTS

IN-AIR, UNSHIELDED
EFFECTIVE CROSS SECTIONS AND REACTION RATES
AT 3 m FROM CENTER OF SHEBA

Detector Component	Effective Cross-section $\bar{\sigma}$ (cm^2)	Energy Range	Reaction Rate ($\bar{\sigma} \times 10^{10}$ Atoms / kW-Min)
Bare Gold	1.07×10^{-22}	Thermal	2.5×10^{-4}
Cadmium-Covered Gold	1.55×10^{-21}	Epi-Thermal 0.62-10 eV	3.2×10^{-4}
Bare Indium	1.96×10^{-22}	Thermal	4.3×10^{-4}
Cadmium-Covered Indium (n,γ)	2.60×10^{-21}	Epi-Thermal 0.62-2 eV	6.4×10^{-4}
Cadmium-Covered Copper	2.55×10^{-25}	10^{-5}-1MeV	2.0×10^{-6}
Cadmium-Covered Indium (n,n')	2.50×10^{-25}	1-9 MeV	1.3×10^{-6}
Sulfur	2.80×10^{-25}	2.9-9 MeV	5.5×10^{-7}

TABLE XI

EXPERIMENT NUMBER 4: LACD COMPONENTS

IN-AIR, UNSHIELDED
EFFECTIVE CROSS SECTIONS AND REACTION RATES
AT 3 m FROM CENTER OF SHEBA

Detector Component	Effective Cross-section $\bar{\sigma}(cm^2)$	Energy Range	Reaction Rate $\left(\frac{\phi\bar{\sigma} \times 10^{10} \text{ Atoms}}{\text{kW-Min}}\right)$
Bare Indium	1.96×10^{-22}	Thermal	4.7×10^{-4}
Cadmium Covered Indium (n,Y)	2.60×10^{-21}	Epi-Thermal 0.62-2 eV	6.5×10^{-4}
Cadmium-Covered Copper	2.55×10^{-21}	10^{-5}-1 MeV	2.4×10^{-6}
Cadmium-Covered Indium (n,n')	2.50×10^{-25}	1-9 MeV	1.1×10^{-6}
Sulfur	2.80×10^{-25}	2.9-9 MeV	3.0×10^{-7}

TABLE XII

AVERAGE REACTION RATES FOR UNSHIELDED, IN-AIR, LACD AND PND PACKETS at 3 m FROM CENTER OF SHEBA

Detector Component	Average of All LACD and PND Packets	Reaction Rates $\pm 1\sigma$ $\frac{\phi\bar{\sigma} \times 10^{10} \text{ Atoms}}{\text{kW-Min}}$		
		LACD Average	PND Average	Ratio of PND Reaction Rate To LACD Reaction Rate
Bare Gold	$3.0 \pm 0.6 \times 10^{-4}$	$3.0 \pm 0.6 \times 10^{-4}$	-	-
Cadmium-Covered Gold	$3.2 \pm 0.6 \times 10^{-4}$	$3.2 \pm 0.6 \times 10^{-4}$	-	-
Bare Indium	$4.9 \pm 1.0 \times 10^{-4}$	$5.3 \pm 0.9 \times 10^{-4}$	$4.2 \pm 0.8 \times 10^{-4}$	0.8
Cadmium-Covered Indium (n,Y)	$5.7 \pm 0.9 \times 10^{-4}$	$5.7 \pm 0.9 \times 10^{-4}$	$5.8 \pm 1.1 \times 10^{-4}$	1.0
Cadmium-Covered Copper	$1.9 \pm 0.3 \times 10^{-6}$	$1.8 \pm 0.3 \times 10^{-6}$	$2.1 \pm 0.4 \times 10^{-6}$	1.2
Cadmium-Covered Indium (n,n')	$1.3 \pm 0.2 \times 10^{-6}$	$1.3 \pm 0.2 \times 10^{-6}$	$1.1 \pm 0.1 \times 10^{-6}$	0.8
Sulfur	$4.8 \pm 0.9 \times 10^{-7}$	$4.6 \pm 1.1 \times 10^{-7}$	$5.3 \pm 0.3 \times 10^{-7}$	1.2

TABLE XIII

IN-AIR, UNSHIELDED NEUTRON-GAMMA DOSE RATIOS

Experiment Number	Dosimeter Type	Source-to-Dosimeter Distance (m)	D_n Neutron Absorbed Dose (rad)	D_γ Gamma Dose (rad)	D_n/D_γ
1	LACD	3	191	135	1.4
2	LACD	3	230	184	1.3
3	LACD	3	456	354	1.3
	PND	2	855		
4	LACD	4.6	191	137	1.4
	PND	4.2	219		

TABLE XIV

EXPERIMENT NUMBER 1: LACD COMPONENTS
(DOSIMETER IN-AIR, 12-cm LUCITE SHIELD)

EFFECTIVE CROSS SECTIONS AND REACTION RATES
AT 3 m FROM CENTER OF SHEBA

Detector Component	Effective Cross-section $\bar{\sigma}(cm^2)$	Energy Range	Reaction Rate $\left(\frac{\phi\bar{\sigma} \times 10^{10} \text{ Atoms}}{kW\text{-Min}}\right)$
Bare Gold	1.07×10^{-22}	Thermal	1.6×10^{-4}
Cadmium-Covered Gold	1.55×10^{-21}	Epi-Thermal 0.62-10 eV	8.5×10^{-5}
Bare Indium	1.96×10^{-22}	Thermal	4.0×10^{-4}
Cadmium-Covered Indium (n,γ)	2.60×10^{-21}	Epi-Thermal 0.62-2 eV	1.6×10^{-4}
Cadmium-Covered Copper	3.83×10^{-25}	10^{-5}-1 MeV	6.2×10^{-7}
Cadmium-Covered Indium (n,n')	2.15×10^{-25}	1-9 MeV	3.0×10^{-7}
Sulfur	1.87×10^{-25}	2.9-9 MeV	8.9×10^{-8}

TABLE XV

EXPERIMENT NUMBER 3: LACD COMPONENTS
(DOSIMETER IN-AIR, 20-cm CONCRETE SHIELD)

EFFECTIVE CROSS SECTIONS AND REACTION RATES
AT 3 m FROM CENTER OF SHEBA

Detector Component	Effective Cross-section $\sigma(cm^2)$	Energy Range	Reaction Rate $\left(\frac{0\bar{\sigma} \times 10^{10} \text{ Atoms}}{kW\text{-Min}}\right)$
Bare Gold	1.07×10^{-22}	Thermal	2.5×10^{-4}
Cadmium-Covered Gold	1.55×10^{-21}	Epi-Thermal 0.62-10 eV	1.5×10^{-4}
Bare Indium	1.96×10^{-22}	Thermal	4.3×10^{-4}
Cadmium-Covered Indium (n,)	2.60×10^{-21}	Epi-Thermal 0.62-2 eV	2.7×10^{-4}
Cadmium-Covered Copper	5.65×10^{-25}	10^{-5}-1MeV	8.5×10^{-7}
Cadmium-Covered Indium (n,n')	2.43×10^{-25}	1-9 MeV	3.1×10^{-7}
Sulfur	2.35×10^{-25}	2.9-9 MeV	1.0×10^{-7}

TABLE XVI

EXPERIMENT NUMBER 4: LACD COMPONENTS
(DOSIMETER IN-AIR, 15-cm STEEL SHIELD)

EFFECTIVE CROSS SECTIONS AND REACTION RATES
AT 3 m FROM CENTER OF SHEBA

Detector Component	Effective Cross-section $\bar{\sigma}$ (cm^2)	Energy Range	Reaction Rate $\left(\frac{0\bar{\sigma} \times 10^{10} \text{ Atoms}}{kW\text{-Min}}\right)$
Bare Gold	1.07×10^{-22}	Thermal	1.7×10^{-5}
Cadmium-Covered Gold	1.55×10^{-21}	Epi-Thermal 0.62-10 eV	2.4×10^{-5}
Bare Indium	1.96×10^{-22}	Thermal	3.7×10^{-5}
Cadmium-Covered Indium (n,γ)	2.60×10^{-21}	Epi-Thermal 0.62-2 eV	3.5×10^{-5}
Cadmium-Covered Copper	3.56×10^{-25}	10^{-5}-1MeV	2.1×10^{-7}
Cadmium-Covered Indium (n,n')	1.95×10^{-25}	1-9 MeV	1.5×10^{-7}
Sulfur	2.93×10^{-25}	2.9-9 MeV	2.9×10^{-8}

TABLE XVII

IN-AIR, SHIELDED NEUTRON-TO-GAMMA DOSE RATIOS

Experiment Number	Source-to-Dosimeter Distance (m)	D_n Neutron Absorbed Dose (rad)	D_γ Gamma Dose (rad)	D_n/D_γ
1	3	59	93	0.6
3	3	105	100	1.1
4	4.6	46	9.8	4.7

TABLE XVIII

DOSE ATTENUATION FACTORS FOR
SHIELDS USED IN EXPERIMENTS 1, 3, AND 4

Experiment Number	Source-to-Dosimeter Distance (m)	$\left(\frac{D_n \text{ Shielded}}{D_n \text{ Unshielded}}\right)$
1	3	0.31
3	3	0.23
4	4.6	0.24

TABLE XIX

EXPERIMENT NUMBER 1: PND COMPONENTS
(PND LOCATION: PHANTOM CHEST)

EFFECTIVE CROSS SECTIONS AND REACTION RATES
AT 3 m FROM CENTER OF SHEBA TO DOSIMETER

Detector Component	Effective Cross-section $\bar{\sigma}$ (cm^2)	Energy Range	Reaction Rate $\left(\frac{0\bar{\sigma} \times 10^{18} \text{ Atoms}}{\text{kW-Min}}\right)$
Bare Indium	1.96×10^{-22}	Thermal	3.8×10^{-4}
Cadmium-Covered Indium (n,γ)	2.60×10^{-21}	Epi-Thermal 0.62-2 eV	1.3×10^{-4}
Cadmium-Covered Copper	3.83×10^{-25}	10^{-5}-1 MeV	6.2×10^{-7}
Cadmium-Covered Indium (n,n')	2.15×10^{-25}	1-9 MeV	3.3×10^{-7}
Sulfur	1.87×10^{-25}	2.9-9 MeV	8.9×10^{-8}

TABLE XX

EXPERIMENT NUMBER 1: PND COMPONENTS (PND LOCATION: PHANTOM BACK)

EFFECTIVE CROSS SECTIONS AND REACTION RATES
AT 3.2 m FROM CENTER OF SHEBA TO DOSIMETER

Detector Component	Effective Cross-section $\sigma(cm^2)$	Energy Range	Reaction Rate $\left(\frac{\bar{\sigma} \times 10^{10} \text{ Atoms}}{\text{kW-Min}}\right)$
Bare Indium	1.96×10^{-22}	Thermal	1.3×10^{-4}
Cadmium-Covered Indium (n,γ)	2.60×10^{-21}	Epi-Thermal 0.62-2 eV	4.9×10^{-5}
Cadmium-Covered Copper	3.83×10^{-25}	10^{-5}-1 MeV	2.0×10^{-7}
Cadmium-Covered Indium (n,n')	2.15×10^{-25}	1-9 MeV	4.7×10^{-8}
Sulfur	1.87×10^{-25}	2.9-9 MeV	1.7×10^{-8}

TABLE XXI

EXPERIMENT NUMBER 2: PND COMPONENTS (PND LOCATION: PHANTOM CHEST)

EFFECTIVE CROSS SECTIONS AND REACTION RATES
AT 3 m FROM CENTER OF SHEBA TO DOSIMETER

Detector Component	Effective Cross-section $\bar{\sigma}\ (cm^2)$	Energy Range	Reaction Rate $\left(\frac{\bar{\sigma} \times 10^{10} \text{ Atoms}}{\text{kW-Min}}\right)$
Bare Indium	1.96×10^{-22}	Thermal	1.3×10^{-3}
Cadmium-Covered Indium (n,γ)	2.60×10^{-21}	Epi-Thermal 0.62-2 eV	7.8×10^{-4}
Cadmium-Covered Copper	2.55×10^{-25}	10^{-5}-1 MeV	2.4×10^{-6}
Cadmium-Covered Indium (n,n')	2.50×10^{-25}	1-9 MeV	9.0×10^{-7}
Sulfur	2.80×10^{-25}	2.9-9 MeV	4.8×10^{-7}

TABLE XXII

EXPERIMENT NUMBER 2: PND COMPONENTS (PND LOCATION: PHANTOM SIDE)

EFFECTIVE CROSS SECTIONS AND REACTION RATES
AT 3.1 m FROM CENTER OF SHEBA TO DOSIMETER

Detector Component	Effective Cross-section $\bar{\sigma}$ (cm^2)	Energy Range	Reaction Rate ($\frac{\phi\bar{\sigma} \times 10^{10} \text{ Atoms}}{kW\text{-}Min}$)
Bare Indium	1.96×10^{-22}	Thermal	3.6×10^{-4}
Cadmium-Covered Indium (n, γ)	2.60×10^{-21}	Epi-Thermal 0.62-2 eV	2.9×10^{-4}
Cadmium-Covered Copper	2.55×10^{-25}	10^{-5}-1 MeV	1.3×10^{-6}
Cadmium-Covered Indium (n,n')	2.50×10^{-25}	1-9 MeV	7.8×10^{-7}
Sulfur	2.80×10^{-25}	2.9-9 MeV	3.9×10^{-7}

TABLE XXIII

EXPERIMENT NUMBER 2: PND COMPONENTS (PND LOCATION: PHANTOM BACK)

EFFECTIVE CROSS SECTIONS AND REACTION RATES
AT 3.2 m FROM CENTER OF SHEBA TO DOSIMETER

Detector Component	Effective Cross-section $\bar{\sigma}$ (cm^2)	Energy Range	Reaction Rate ($\frac{\phi\bar{\sigma} \times 10^{10} \text{ Atoms}}{kW\text{-}Min}$)
Bare Indium	1.96×10^{-22}	Thermal	3.3×10^{-4}
Cadmium-Covered Indium (n, γ)	2.60×10^{-21}	Epi-Thermal 0.62-2 eV	3.3×10^{-4}
Cadmium-Covered Copper	2.55×10^{-25}	10^{-5}-1 MeV	6.0×10^{-7}
Cadmium-Covered Indium (n,n')	2.50×10^{-25}	1-9 MeV	1.7×10^{-7}
Sulfur	2.80×10^{-25}	2.9-9 MeV	6.6×10^{-8}

TABLE XXIV

EXPERIMENT NUMBER 3: PND COMPONENTS (PND LOCATION: PHANTOM CHEST)

EFFECTIVE CROSS SECTIONS AND REACTION RATES
AT 3 m FROM CENTER OF SHEBA TO DOSIMETER

Detector Component	Effective Cross-section $\bar{\sigma}$ (cm^2)	Energy Range	Reaction Rate $\left(\frac{\bar{\phi}\bar{\sigma} \times 10^{10} \text{ Atoms}}{\text{kW-Min}}\right)$
Bare Indium	1.96×10^{-22}	Thermal	3.3×10^{-4}
Cadmium-Covered Indium (n, γ)	2.60×10^{-21}	Epi-Thermal 0.62-2 eV	2.5×10^{-4}
Cadmium-Covered Copper	5.65×10^{-25}	10^{-5}-1 MeV	8.3×10^{-7}
Cadmium-Covered Indium (n,n')	2.43×10^{-25}	1-9 MeV	2.1×10^{-7}
Sulfur	2.35×10^{-25}	2.9-9 MeV	1.1×10^{-7}

TABLE XXV

EXPERIMENT NUMBER 3: PND COMPONENTS (PND LOCATION: PHANTOM SIDE)

EFFECTIVE CROSS SECTIONS AND REACTION RATES
AT 3.1 m FROM CENTER OF SHEBA TO DOSIMETER

Detector Component	Effective Cross-section $\bar{\sigma}$ (cm^2)	Energy Range	Reaction Rate $\left(\frac{\bar{\phi}\bar{\sigma} \times 10^{10} \text{ Atoms}}{\text{kW-Min}}\right)$
Bare Indium	1.96×10^{-22}	Thermal	2.9×10^{-4}
Cadmium-Covered Indium (n, γ)	2.60×10^{-21}	Epi-Thermal 0.62-2 eV	1.8×10^{-4}
Cadmium-Covered Copper	5.65×10^{-25}	10^{-5}-1 MeV	7.1×10^{-7}
Cadmium-Covered Indium (n,n')	2.43×10^{-25}	1-9 MeV	2.0×10^{-7}
Sulfur	2.35×10^{-25}	2.9-9 MeV	9.5×10^{-8}

TABLE XXVI

EXPERIMENT NUMBER 3: PND COMPONENTS (PND LOCATION: PHANTOM BACK)

EFFECTIVE CROSS SECTIONS AND REACTION RATES
AT 3.2 m FROM CENTER OF SHEBA TO DOSIMETER

Detector Component	Effective Cross-section $\bar{\sigma}$ (cm^2)	Energy Range	Reaction Rate $\left(\frac{\bar{\phi\sigma} \times 10^{10} \text{ Atoms}}{\text{kW-Min}}\right)$
Bare Indium	1.96×10^{-22}	Thermal	1.5×10^{-4}
Cadmium-Covered Indium (n, γ)	2.60×10^{-21}	Epi-Thermal 0.62-2 eV	8.3×10^{-5}
Cadmium-Covered Copper	5.65×10^{-25}	10^{-5}-1 MeV	3.0×10^{-7}
Cadmium-Covered Indium (n,n')	2.43×10^{-25}	1-9 MeV	8.1×10^{-8}
Sulfur	2.35×10^{-25}	2.9-9 MeV	3.1×10^{-8}

TABLE XXVII

EXPERIMENT NUMBER 3: PND COMPONENTS (PND LOCATION: PHANTOM CHEST)

EFFECTIVE CROSS SECTIONS AND REACTION RATES
AT 4.6 m FROM CENTER OF SHEBA TO DOSIMETER

Detector Component	Effective Cross-section $\bar{\sigma}$ (cm^2)	Energy Range	Reaction Rate $\left(\frac{\bar{\phi\sigma} \times 10^{10} \text{ Atoms}}{\text{kW-Min}}\right)$
Bare Indium	1.96×10^{-22}	Thermal	1.4×10^{-4}
Cadmium-Covered Indium (n,γ)	2.60×10^{-21}	Epi-Thermal 0.62-2 eV	8.9×10^{-5}
Cadmium-Covered Copper	3.56×10^{-25}	10^{-5}-1 MeV	2.5×10^{-7}
Cadmium-Covered Indium (n,n')	1.95×10^{-25}	1-9 MeV	6.6×10^{-8}
Sulfur	2.93×10^{-25}	2.9-9 MeV	1.4×10^{-8}

TABLE XXVIII

EXPERIMENT NUMBER 4: PND COMPONENTS (PND LOCATION: PHANTOM SIDE)

EFFECTIVE CROSS SECTIONS AND REACTION RATES
AT 4.7 m FROM CENTER OF SHEBA TO DOSIMETER

Detector Component	Effective Cross-section $\bar{\sigma}$ (cm^2)	Energy Range	Reaction Rate $\left(\frac{\bar{\sigma}\phi \times 10^{10} \text{ Atoms}}{\text{kW-Min}}\right)$
Bare Indium	1.96×10^{-22}	Thermal	1.0×10^{-4}
Cadmium-Covered Indium (n,γ)	2.60×10^{-21}	Epi-Thermal 0.62-2 eV	5.3×10^{-5}
Cadmium-Covered Copper	3.56×10^{-25}	10^{-5}-1 MeV	2.6×10^{-7}
Cadmium-Covered Indium (n,n')	1.95×10^{-25}	1-9 MeV	5.3×10^{-8}
Sulfur	2.93×10^{-25}	2.9-9 MeV	1.4×10^{-8}

TABLE XXIX

EXPERIMENT NUMBER 4: PND COMPONENTS (PND LOCATION: PHANTOM BACK)

EFFECTIVE CROSS SECTIONS AND REACTION RATES
AT 4.8 m FROM CENTER OF SHEBA TO DOSIMETER

Detector Component	Effective Cross-section $\bar{\sigma}$ (cm^2)	Energy Range	Reaction Rate $\left(\frac{\bar{\sigma}\phi \times 10^{10} \text{ Atoms}}{\text{kW-Min}}\right)$
Bare Indium	1.96×10^{-22}	Thermal	6.9×10^{-5}
Cadmium-Covered Indium (n,γ)	2.60×10^{-21}	Epi-Thermal 0.62-2 eV	2.8×10^{-5}
Cadmium-Covered Copper	3.56×10^{-25}	10^{-5}-1 MeV	1.2×10^{-7}
Cadmium-Covered Indium (n,n')	1.95×10^{-25}	1-9 MeV	1.4×10^{-8}
Sulfur	2.93×10^{-25}	2.9-9 MeV	1.1×10^{-8}

TABLE XXX

NEUTRON AND GAMMA DOSES TO PHANTOM

Experiment Number	PND Phantom Location	Phantom PND Neutron Absorbed Dose (rad)[a]	LACD In-Air Neutron Absorbed Dose (rad)[a]	Gamma Dose (rad)
1	Chest	54	59	110
	Back	13		55
2	Chest	201	230	195
	Side	112		-
	Back	44		113
3	Chest	91	105	123
	Side	79		105
	Back	32		68
4	Chest	43	46	18
	Side	28		14
	Back	12		12

[a]SHEBA-to-dosimeter distance per Table II.

TABLE XXXI

RATIO OF PHANTOM SIDE AND BACK TO CHEST DOSES (NEUTRON AND GAMMA)

Experiment Number	D_n Back / D_n Chest	D_n Side / D_n Chest	D_γ Back / D_γ Chest	D_γ Side / D_γ Chest
1	0.24	-	0.50	-
2	0.22	0.56	0.58	-
3	0.35	0.87	0.55	0.85
4	0.27	0.66	0.68	0.78

TABLE XXXII

BLOOD-SODIUM ANALYSIS RESULTS

Experiment Number	Configuration	^{24}Na Activity (μCi ^{24}Na/mg ^{23}Na)	Sulfur Fluence to Sodium Activation[a] (n/cm^2) Per (μCi ^{24}Na/mg ^{23}Na)	Blood-sodium[b] Neutron Absorbed Dose Estimate (rad)	LACD Neutron Absorbed Dose Estimate (rad)
1	12-cm Lucite Shield Phantom Chest at 3 m	1.1×10^{-4}	3.4×19^{13}	59	59
2	Unshielded Phantom Chest at 3 m	8.1×10^{-4}	1.7×10^{13}	222	230
3	20-cm Concrete Shield Phantom Chest at 3 m	3.3×10^{-5}	2.0×10^{14}	95	105
4	15-cm Steel Shield Phantom Chest at 8.6 m	1.5×10^{-4}	1.0×10^{13}	45	46

[a]Sulfur fluences determined with LACD sulfur tablets.

[b]Dose estimates determined from Fig. 4 of Ref. 8.

TABLE XXXIII

COMPARISON OF LACD DOSE ESTIMATES TO BLOOD-SODIUM DOSE ESTIMATES AND LACD DOSE ESTIMATES TO PND DOSE DETERMINATIONS

Experiment Number	Ratio of LACD Dose To Blood-Sodium Dose (Absorbed)	Ratio of LACD Absorbed Dose to PND Absorbed Dose Measured on Chest of Phantom
1	1.00	0.91
2	1.04	0.87
3	1.11	0.87
4	1.03	0.92

TABLE XXXIV

SUMMARY OF GEIGER COUNTER ANALYSES OF INDIUM FOILS IN PND DOSIMETER (AVERAGE MASS OF BARE INDIUM FOIL IN PNDs IS 0.236 g)

Experiment Number	Configuration	PND Location on Phantom	Geiger-Counter Dose-Rate[a] Per rad Neutron ($mR/hr\text{-}rad_n$)	Dose-Rate Per rad Neutron at Each Location/Dose-Rate Per rad Neutron To Chest of Phantom
1	12-cm Lucite Shield	Chest	3.9×10^{-1}	1.00
		Back	1.4×10^{-1}	.35
2	Unshielded	Chest	8.5×10^{-1}	1.00
		Side	3.3×10^{-1}	.39
		Back	2.3×10^{-1}	.27
3	20-cm Concrete	Chest	1.3×10^{0}	1.00
		Side	8.6×10^{-1}	.69
		Back	3.7×10^{-1}	.30
4	15-cm Steel	Chest	7.0×10^{-1}	1.00
		Side	4.9×10^{-1}	.70
		Back	3.0×10^{-1}	.43

[a]Corrected to the end of exposure.

REFERENCES

1. C. S. Sims and R. E. Swaja, "Sixteenth Nuclear Accident Dosimetry Intercomparison Study: August 13-17, 1979," Oak Ridge National Laboratory report ORNL/TM-7596 (December 1980).

2. D. G. Vasilik and R. W. Martin, "The Los Alamos Personnel and Area Criticality Dosimeter Systems," Los Alamos National Laboratory report LA-8848-MS (June 1981).

3. International Atomic Energy Agency, "Nuclear Accident Dosimetry Systems" (IAEA, Vienna, 1970), 181.

4. D. E. Hankins, "A Study of Selected Criticality-Dosimetry Methods," Los Alamos National Laboratory report LA-3910 (June 1968).

5. D. F. Peterson, V. E. Mitchell, and W. H. Langham, "Estimation of Fast Neutron Doses in Man by ^{32}S (n,p) and ^{32}P Reaction in Body Hair," Health Phys. 6, 1 (1961).

6. D. F. Peterson and W. H. Langham, "Neutron Activation of Sulfur in Hair: Application in a Nuclear Accident Dosimetry Study," Health Phys. 12, 381 (1966).

7. D. E. Hankins, "Direct Counting of Hair Samples for ^{32}P Activation," Health Phys. 17, 740 (1969).

8. D. E. Hankins, "Dosimetry of Criticality Accident Using Activations of the Blood and Hair," Health Phys. 38, 529 (1980).

9. H. M. Murphy, "Summary of Neutron and Gamma Dosimetry Techniques," Air Force Weapons Laboratory report, Kirtland Air Force Base,AFWL-TR-66-111, (September 1967).

10. H. Ing and S. Makra, "Compendium of Neutron Spectra in Criticality Accident Dosimetry," Technical Report Series No. 180 (IAEA, Vienna, 1978).

11. J. A. Auxier, W. S. Snyder, and T. D. Jones, "Neutron Interactions and Penetration in Tissue," in Radiation Dosimetry, F. H. Attix and W. C. Roesch (Eds.), 2nd edition (New York, Academic Press, 1968), Ch. 6.

12. National Council on Radiation Protection and Measurements, "Protection Against Neutron Radiation up to 30 Million Electron Volts," Natl. Bur. Std. (US) Handbook 63.

13. M. S. Singh, "Kerma Factors for Neutrons and Photons with Energies Below 20 MeV," University of California Lawrence Radiation Laboratory report UCRL-52850 (1979).

14. J. Palfavi and L. Koblinger, "Spectra of Neutrons Transmitted through and Reflected from Different Homogeneous Slabs," Hungarian Academy of Sciences report KFKI-76-58 (Central Research Institute for Physics, Budapest, 1976).

15. G. P. de Beer, "Differential Neutron Albedos for Cylindrical Water Surfaces," Nucl. Eng. and Design, 33, 422 (1975).

16. R. E. Maerker and F. J. Muckenthaler, "Calculations and Measurement of the Fast-Neutron Differential Dose Albedo for Concrete," Nucl. Sci. Eng. 22, 455 (1965).

17. R. G. Jaeger, Ed., Engineering Compendium on Radiation Shielding, Vol. I, (Springer-Verlag, New York, 1968).

18. K. Becker, Solid State Dosimetry (CRC Press, Cleveland, Ohio, 1973).

19. US Department of Energy, "Nuclear Accident Dosimetry Program, Manual 0545 (May 2, 1974).

20. American National Standards Institute, "Dosimetry of Criticality Accidents," ANSI N13.3-1969 (1969).